Small Structures

small structures

www.small-structures.com

RESEARCH ARTICLE OPEN ACCESS

Gold Nanoparticle Melting: Effects of Size, Support Interaction, and Orientation

Th. Pavloudis[1,2,3] | C. Gennetidis[2,4] | J. Kioseoglou[2,3] | R. E. Palmer[1]

[1]Nanomaterials Lab, Mechanical Engineering, Swansea University, Bay Campus, Fabian Way, Swansea, United Kingdom | [2]School of Physics, Aristotle University of Thessaloniki, A.U.Th. Campus, Thessaloniki, Greece | [3]Center for Interdisciplinary Research and Innovation, Aristotle University of Thessaloniki, Balkan Center, Buildings A and B, 10th km Thessalonikis -Thermis, Thessaloniki, Greece | [4]INSA Lyon, University of Lyon, Villeurbanne, France

Correspondence: Th. Pavloudis (tpavlo@auth.gr)

Received: 31 August 2025 | **Revised:** 17 November 2025 | **Accepted:** 3 December 2025

Keywords: force fields | gold | machine learning | melting | nanoclusters | nanoparticles

ABSTRACT

An understanding of nanoparticle (NP) melting is essential for both fundamental nanoscience and the design of high-temperature catalytic systems. We investigate the melting behavior of truncated octahedral gold NPs, ranging in size from 2 to 4 nm, supported on their edges, (100) or (111) facets, using molecular dynamics simulations, with a machine-learning force field trained on density functional theory data. We systematically examine the effects of NP size, support interactions, and orientational dependence by applying spring-like constraints to specific facets or edges. Our results show that NP melting follows the liquid nucleation and growth model, with surface disorder preceding rapid melting at a critical temperature. Constraining the atoms to simulate contact with a support consistently raises the melting temperature, with stronger effects for smaller clusters, and for (100) facets compared with (111) facets, that is, there is an orientational effect. Importantly, the extent of the offset in melting temperature is quite independent of the interaction strength, implying that all support interactions can significantly stabilize small NPs. These findings provide a framework for more accurate predictions of nanoscale melting in practical catalytic environments.

1 | Introduction

Nanoparticles (NPs), and particularly Au NPs, have been the focus of nanoscience for decades both as a model material, but also due to their unique catalytic behavior [1]. The seminal work of Haruta et al. on sub-5 nm Au NPs [2] proved that the smallest of NPs exhibited 'boosted' activity. Since catalytic devices usually operate at elevated temperatures, a thorough understanding of the behavior of these small particles at these temperatures and the mechanisms governing their melting is essential for the development, manufacturing, and processing of new catalytic systems.

Since the early days of nanoscience, researchers have proposed various models to predict NP melting. At the beginning of the 20th century, Pawlow [3] introduced a model based on the triple-point equilibrium of spherical solid and liquid particles of the same material and mass, surrounded by their vapor. This model predicted a $1/r$ dependence of the melting temperature on the NP radius r. Much later, Reiss and Wilson [4], Hanszen [5], Curzon [6], and Sambles [7] developed the liquid shell model, which posits a solid core surrounded by a liquid shell of constant thickness near the melting temperature. Shortly after, Couchman and Jesser [8], proposed the liquid nucleation and growth (LNG) model, rooted in nucleation theory, in which melting begins with the nucleation of a liquid shell at the NP surface. This shell then grows inward until a critical radius is reached, at which point the entire particle melts. This model thus predicts a melting region characterized by solid–liquid coexistence. These theories, however, treat the particle as a continuum and therefore cannot resolve atomic-level effects of shape, faceting, alloying, defects, or support interactions.

The $1/r$ dependence of the melting temperature and the existence of a liquid shell prior to melting has been experimentally confirmed for both small and large Au NPs using in situ heating stages and high-resolution transmission electron microscopes (TEM) [9] or aberration-corrected scanning TEMs [10, 11]. In the later study, the observed $1/r$ dependence of surface and NP melting temperatures matched theoretical predictions, but at significantly higher temperatures than those predicted by existing models. Large-scale ab initio molecular dynamics (MD) simulations, in which one of the NP facets was 'frozen' to account for the influence of the support on NP melting, revealed that the discrepancy arises from this previously overlooked effect. Other recent MD simulations coupled with crystallinity analysis algorithms reaffirmed that the LNG model can describe the melting of monometallic NPs of large sizes [12].

Together with size, structure, and composition, NP-support interactions are known to influence the behavior of nanocatalysts [13]. A wealth of theoretical studies has shown that these interactions are strong enough to dominate the morphology, kinetics, and stability of small NPs [14]. While different metals will exhibit different metal–support interactions with different supports, previous works on platinum group metals (PGMs) have yielded supporting results. For example, melting was found to start at the NP-support interface for Ag NPs on SiO_2 [15]. In Pt NPs on MgO(100), the support caused NP wetting, determined crystal structure and stabilized the NP against solid–liquid transition [16]. NP morphology was also found to be support dependent for Pt NPs on carbon supports [17, 18]. Importantly, in the former work, the melting temperature was shown to depend strongly on NP size, but weakly on the specific features of the support. The melting temperature of ~6 nm Cu NPs on graphene was found to decrease with an increasing NP–substrate interaction strength, which was shown to destabilize the NP [19].

Hints of an orientational dependence of NP dynamics were recently reported: small Pt particles were shown to prefer 3D shapes on CeO_2(111) facets, but 2D raft structures on CeO_2(100) facets, and were recorded in real time to undergo a 3D to 2D dimensionality change when migrating from CeO_2(111) to CeO_2(100) [20]. Recently, graphene/Ni(111) supports were shown to reshape Ag NPs between 1.5 and 6.5 nm [21]. The authors concluded that widely used shape construction methods need to updated for NPs below 5 nm.

Au has exhibited unique catalytic properties, that differ from those of other PGM NPs. The unique catalytic abilities of Au NPs strongly depend on their size, and importantly, their interface with the support [22]. Previously, a graphitic carbon support was shown to rule the formation and breaking of synapses between large Au_{1415} NPs at elevated temperature [23]. Experimentally, interactions with the carbon support were shown to stabilize 2D structural motifs of small Au particles of way bigger sizes compared to previous theoretical predictions for free NPs [24]. 2–3 nm Au NPs in the pores mesoporous silica showed high thermal stability, even at ~700–800°C, leading to very active but also very stable catalysts [25].

Various modeling methods, each with its own advantages and disadvantages, have been used to model NP melting. Mesoscopic descriptions (e.g. phase-field models) can incorporate realistic geometries and interfacial energetics but still rely on effective parameters that must be obtained from experiment. Classical MD with empirical potentials (Lennard–Jones, EAM/MEAM, Sutton–Chen, Gupta, and so on) resolve the melting process at the atomic scale, capturing surface premelting, solid–liquid coexistence, and nonspherical shapes, at the cost of a strong dependence on the chosen interatomic potential and its accuracy. Recent machine-learned interatomic potentials provide near first-principles accuracy for NPs containing thousands of atoms, at the expense of a more involved training and validation procedure.

In this work, we present a more comprehensive computational study of supported Au NPs than previously reported, that is, a more sophisticated version of the 'frozen facet' approach first presented in Ref. [11]. Specifically, we constrain the cluster atoms in contact with the support in a more subtle manner compared to the previous work. We employ MD simulations to investigate atomic-scale factors influencing the melting process, including NP size, adhesion to the substrate, and landing orientation. We use a recently developed machine-learning force field for Au, trained on density functional theory (DFT) data, which accurately reproduces the melting points of small NPs and captures surface melting phenomena [26]. To model the NP–support interactions, we constrain specific regions of the NP with springs of varying stiffness. Our results thus elucidate the effects of the cluster size, the strength of the NP–support interaction, and the NP orientation (i.e which facet sits on the substrate support) on the melting mechanism. The scale of these effects can be substantial, raising the melting point by tens of degrees K.

2 | Theoretical Details

The simulations in this work were performed with the LAMMPS [27] MD simulator using the FLARE [28] add-on. A machine learning force fields (ML-FF) potential [26] trained on data gathered from DFT calculations was used. Out of the three ML-FF potentials created in Ref. [26], the hybrid version, which is a linear combination of the 2- and 3-body FFs of the ML-FFs derived from DFT calculations using local density approximation [29] and revised Perdew–Burke–Ernzerhof [30] functionals, was chosen for this work. This hybrid version of the ML-FF showed a cohesive energy in the bulk phase that matched the experimental one and NP melting temperatures within 50 K from the melting temperatures found experimentally [26].

The temperature of the system was controlled using a Nose–Hoover thermostat with a 5 fs time step. The temperature continuously increased at a rate of 20 K/ns, with starting temperatures at 300 K and ending temperatures that ranged between 1000 and 1400 K, depending on the size of the NPs. The simulation duration ranged from 39 to 63 ns for the smallest and largest NPs, respectively. The time step and heating rate were copied from Ref. [26]. In this work, the evolution of NPs ranging from 147 to 6266 atoms between 400 and 1600 K was thoroughly sampled for different heating rates, and no observable difference in the T_m was found between 5, 10, and 20 K/ns. The authors concluded that any superheating effects are not strongly affecting the T_m estimates.

The model NPs were created from truncations of face-centered cubic (FCC) crystalline Au blocks. These crystalline NPs comprise both (100) and (111) facets of varying relative sizes. If a is the number of atoms on the edges of the (100) facets and b is the number of atoms on the edges of the (111) facets (Figure S1a),

then $a = 1$ results to no (100) facets, that is, octahedrons, and $a = b$ results to (100) and (111) facets of equal dimensions, that is, cuboctahedrons. To find the energetically preferable structural motifs, we built and relaxed using the hybrid version of the ML-FF potential from Ref. [26] octahedral NPs ($a = 1$), cuboctahedral ($a = b$), and truncated octahedral NPs of various truncations ($b = a + 2$, $b = a + 4$, $b = a + 6$, and $b = a + 8$). We found that NPs that belong to the $b = a + 2$ and $b = a + 4$ families were of the higher stability for the size regimes that were the focus of this work (Figure S1b). We chose the $b = a + 2$ family for our MD simulations.

Our models consisted of NPs comprising 405, 711, 1139, and 1709 atoms, which correspond to NP diameters from 2.1 to 3.6 nm. These truncated octahedral NPs comprise (100) and (111) facets of tetragonal and convex irregular hexagonal shape, respectively. The size of the (111) facets is always larger compared to the (100) facets. We used two additional large NPs of 2441 and 4229 atoms (4.1 and 5.0 nm in diameter) to extract the bulk melting temperature of Au.

In an effort to investigate and quantify the effect of the support on the melting of the NPs, the simulation approach we followed in this work was based on two sets of MD simulations. In one set, all the atoms of the NP were free to move ('unsupported' clusters). In the other set, springs were applied independently to each of the atoms of one (100) facet of the NP, one (111) facet of the NP and an edge of the NP, to tether them to their initial positions. The three different configurations are shown in Figure 1 and the number of atoms under constraints for each case and size is given in Table S1. This method is a workaround to adding support layers, in order to (i) save computational time, since a realistic support model would add thousands of atoms to the calculation and ML-FFs, if they exist for the element combination under study, are still slow compared to classic MD simulations (e.g. adding 4 graphitic layers for a 100×100 Å box would result in simulations with ~14 k atoms), and (ii) provide the community with a more generalized result, independent of the specifics of the support.

We simulated a soft-landing scenario, where the NPs would only lay on the support and would not be embedded in it. By 'soft landing' we mean a low-energy deposition where the NPs kinetic energy is lower than the binding energy of its constituent atoms. The NPs' morphology is generally preserved in these low-energy impacts. We applied the springs on the bottom layer of NP atoms only, since we had evidence from our previous work on Au NP-graphene support interactions [31] that the forces on the 2nd atomic layer are less than ½ of the forces acting on the 1st atomic layer (Figure S3). A future, more thorough work may apply springs of different k constants on each layer according to the DFT data.

We used three different values for the spring constant k (1, 5, and 10 eV/Å) in order to simulate different bonding strengths between the NP and the support. Figure S2 shows a comparison between the forces on a single Au atom on a defected graphene sheet derived from DFT calculations and the k constants chosen for this work.

There are different ways for the determination of the melting temperature of a NP. One would be to plot the potential energy–temperature curve [32]. Another would be to look into the pair-distance distribution function [33]. We choose to employ a common neighbor analysis (CNA) [34] algorithm using an adaptive cut-off radius [35] through the OVITO visualization and data analysis program [36] in order to extract the degree of crystallinity of the nanocluster as a qualitative measure of the melting process. The melting temperature T_m of the NPs was defined as the point at which the NP's crystallinity becomes zero and all atoms are recognized as amorphous. It should be noted that we count atoms in an FCC arrangement only. The translation between number of atoms and NP size is based on relaxations of semi-spherical icosahedral NPs using the ML-FF potential. The results of these relaxations are listed in Table S2. The diameter estimations of the NPs in this work are given in Table S3.

Two simulations for each specific NP size/facet or edge constrained/k constant combination with slightly different initial velocity distributions were performed. The average critical and NP melting temperatures from the two runs were used for the fitted curves.

3 | Results and Discussion

3.1 | Melting Mechanism

In general, the melting behavior of the NPs was consistent with the predictions of the LNG model. A representative example is shown in Figure 2 for an unsupported Au_{1139} NP. The CNA algorithm identified the outer-layer atoms as noncrystalline due to their insufficient number of nearest neighbors. For the 1139-atom NP, this corresponded to 428 atoms, leaving an initial FCC crystalline count of 711. Between 300 and ~600 K, the NP's crystallinity decreased linearly with increasing temperature. Although the atoms remained largely in their cubic crystalline positions, their bond lengths and angles became increasingly distorted. At this stage, the NP would still be visually recognizable as crystalline octahedral.

Above ~600 K, an increasing number of atoms left their crystalline positions and were classified as amorphous by the CNA algorithm, leading to a steeper decline in crystallinity. The surface became progressively disordered, and by 800 K, the NP already appeared semi-spherical to the eye, albeit having a still large

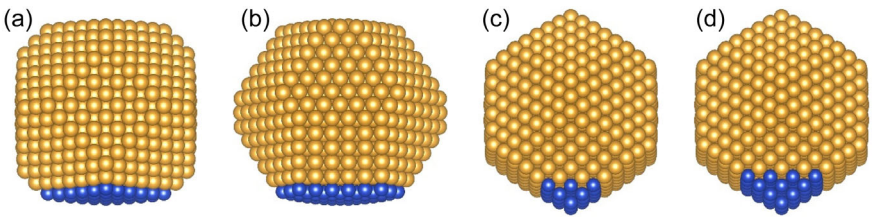

FIGURE 1 | The different areas under constraints in a Au_{1709} nanoparticle: (a) (100) facet, (b) (111) facet, (c) an edge, and (d) a wider edge. Yellow atoms are free to move. Springs are applied to blue atoms.

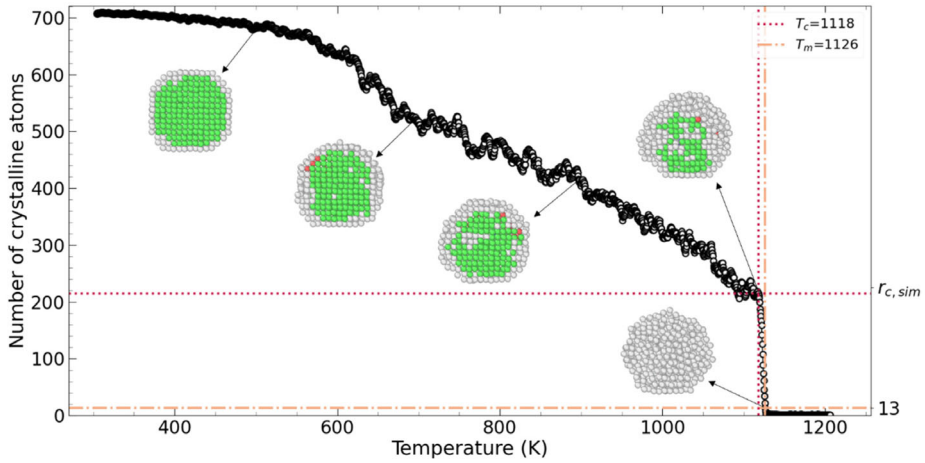

FIGURE 2 | The evolution of the crystallinity of a Au_{1139} NP with the temperature of the simulation. Atoms in green and red were recognized as FCC and HCP, respectively, while atoms in gray were found to be noncrystalline. The critical temperature T_c, the corresponding critical radius r_c, and the melting temperature T_m are noted on the graph.

crystalline core. Melting is a dynamic process. The crystalline core was of an always decreasing but varying size as can be observed by the crystallinity fluctuations in Figure 2. When a facet was constrained, the core was positioned toward this area. Internally, the higher thermal energy caused some atoms to transform into metastable structures, predominantly hexagonal close-packed (HCP), and less frequently, body-centered cubic. In this case, between ~500 K and the critical temperature, a group of ~20–80 atoms persisted in an HCP arrangement. We also observed brief, localized recrystallizations that quickly disappeared.

When a critical temperature T_c was reached—1118 K in this case—the NP underwent a sudden, complete melting. All remaining crystalline atoms became amorphous within a temperature interval of less than ~10 K. The corresponding critical radius r_c, first extracted in number of crystalline atoms and then translated to nm, was in this case 0.83 nm.

In Figure 3, a reel of a Au_{1709} NP supported on its (100) facet near the critical temperature are shown. Initially, a large portion of the atoms of the NP are identified as crystalline. In this supported NP, the solid core of the NPs is of larger size compared than that of an unsupported NP of the same size and is positioned not at the geometric center but shifted toward the restrained region (the bottom atomic layer). However, after only 6 K, the NP is completely amorphous.

3.2 | Size and Orientational Dependence

The melting temperatures T_m of all our models versus the NP size are shown in Figure 4. Extended Freundlich-like power functions provide good fits to our data. We used

$$T_m = T_{m,bulk} \cdot N^{aN^{-b}}$$

where $T_{m,bulk}$ was the bulk melting temperature of Au and N was the number of atoms in our NPs. By fitting on the free NPs, we extracted the $T_{m,bulk}$ for Au, which was found to be 1400 ± 32 K with the ML-FF potential, a slight overestimation of the experimental melting temperature of 1337 K. For consequent fittings, we set $T_{m,bulk}$ at 1400 K and let the a and b parameters free.

Constraining the movement of the facet or edge atoms always hindered NP melting. In all cases, the melting temperature offset was more pronounced in smaller size clusters and was reduced as the NP size increased. For example, the melting of Au_{405} and Au_{1709} NPs were deferred by ~50 K and ~15 K on average, respectively. The rise in melting temperature was projected to be very significant for sub-1 nm NPs, especially if they had a (100) facet or one of their edges in contact with the support. This suggested that these small NPs, which are of significant interest since they lie in the catalytically very active regime, might remain crystalline to temperatures more than 50 K higher than previously expected.

Importantly, regardless of the k constant of the springs, which represents the strength of the interaction with the support, the cluster melting offset was more or less the same. The differences were deemed to be within the statistical error. It appeared that the result was determined only from the group of same atoms are kinetically constrained, and not from the strength of the constraint itself. A similar result was reported in Ref. [37], where the initial state (structures and relative orientations) of colliding 2 nm Au NPs had a persistent influence on the final structure

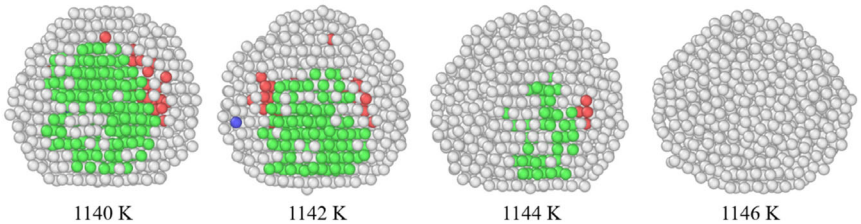

FIGURE 3 | Images of an Au_{1709} nanoparticle showing the rapid melting after the critical radius r_c is reached.

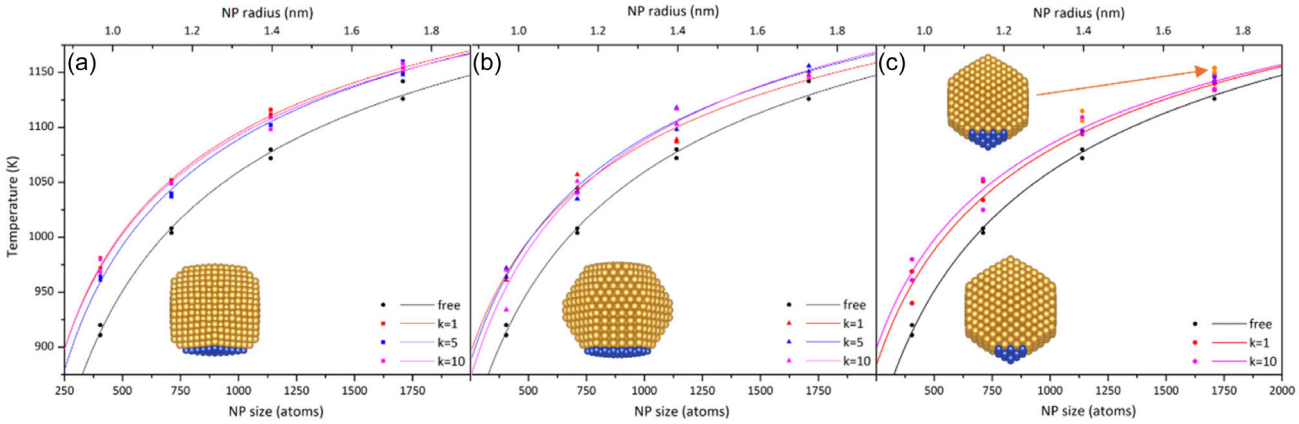

FIGURE 4 | Melting point depression in Au NPs. Springs of constant k are applied (a) to the atoms of a (100) facet, (b) to the atoms of a (111) facet, and (c) to atoms of an edge of the Au NPs.

of the coalesced aggregates, due to a special type of 'kinetic trapping'. It is, hence, expected that the melting of the NP will be hindered even when there are only weak interactions with the support material. Similarly, in Ref. [17], melting temperature of Pt NPs on carbon supports was shown to depend weakly on the support morphology, that is, NP-support bonding configuration.

The *orientational* (i.e. facet) dependence of nanoscale melting is illustrated in Figure 5, where the melting offset $\Delta T = T_{\mathrm{m,constrained}} - T_{\mathrm{m,free}}$ is shown for each case. Interestingly, constraining the (100) facet produced a greater increase in melting point than constraining the (111) facet, even though the (100) facets are smaller in these NPs. Additionally, atoms on the (111) facet have a higher coordination number compared to ones on the (100) facet. The more reactive (100) facet, with its higher number of dangling bonds, is expected to generally anchor more strongly to the support compared to the (111) facet, thereby elevating the Au NP's melting point. The difference between these two cases remains at ~10 K regardless of NP size.

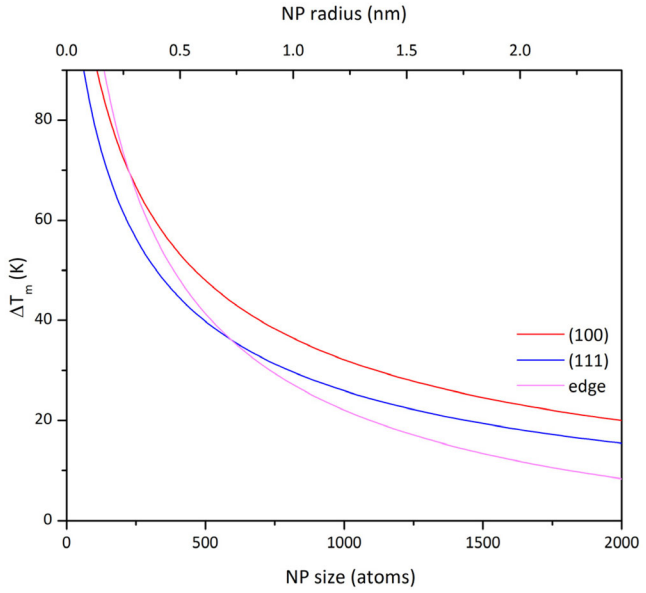

FIGURE 5 | Orientational effects in nanoscale melting: the melting temperature offset depending on the set of atoms interacting with the support.

When the edge is in contact with a support, and for NP radii larger than 1 nm, the melting temperatures show the smallest offset. However, this geometry would only be expected in cluster soft-landing scenarios. Moreover, especially for the larger NPs, only a very small percentage of the atoms are constrained by the support if the cluster binds to the surface edge-on. To test how this holds for wider interactions, we performed additional runs where we applied the constraints to more atoms in the vicinity of the edge (50 vs. 26) to simulate deeper embedding of the NP in the support. This retarded the melting by ~7–10 K more than the original edge-constrained case, suggesting that (as expected) the deeper the NP is embedded in the support, the more pronounced the effect will be. A thorough investigation of embedding depth and its relation to the melting temperature would be of interest for follow-up studies.

3.3 | Critical Radius

The critical radii recorded in this work with the radii of the NPs show a good linear relation (Figure S4). The LNG model critical radius r_c is given by [38]

$$r_{\mathrm{c}} = \frac{2\sigma_{\mathrm{sl}} V_{\mathrm{s}} T_{\mathrm{m,bulk}}}{L\left(T_{\mathrm{m,bulk}} - T\right)} = a \cdot \frac{T_{\mathrm{m,bulk}}}{T_{\mathrm{m,bulk}} - T}$$

where $\sigma_{\mathrm{sl}} = \sigma_{\mathrm{s}} - \sigma_{\mathrm{l}}$, with σ_{s} the surface tension of the solid and σ_{l} the surface tension of the liquid, V_{s} is the molar volume of the solid, L is the molar latent heat, and $T_{\mathrm{m,bulk}}$ is the bulk melting temperature. The values used for plotting the melting models are noted in Table S4. A comparison between the theoretically predicted critical radii, the critical radii and critical temperatures extracted from our calculations and the experimental measurements of the smallest solid core sizes observed in Ref. [9] is shown in Figure 6, where fits according to the above power law are applied.

Both our calculated radii and the experimentally observed radii lied in the region below the curve predicted by the model, which corresponds to the liquid region. We noticed a good agreement of our data with the experimental data, with the exception of the odd point 1.4 nm. The radii for both small and large particles were either very close to our predictions for free NPs (1.1, 1.6, and 2.3 nm) validating the choice of the ML potential, or

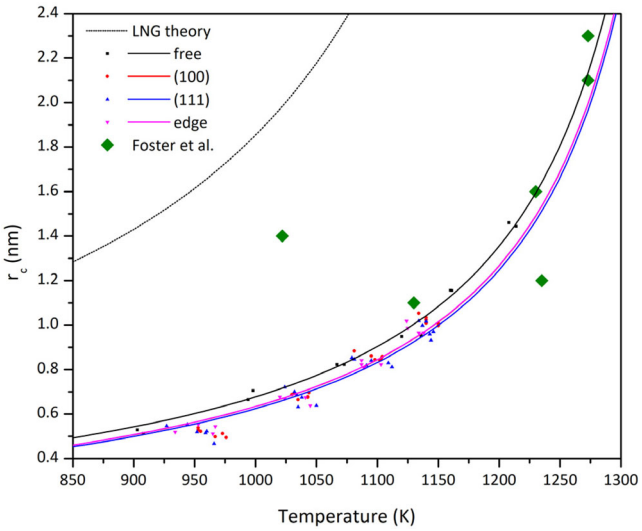

FIGURE 6 | The critical radius predicted by the LNG model compared to the critical radii extracted from the simulations and the experimentally measured smallest solid core radii from Ref. [9]. The fitted curves of (100) and "edge" cases are almost indistinguishable.

close—even below—our predictions for constrained particles (1.2 and 2.1 nm). However, more experimental data of in situ melting of small NPs are in dire need to complement theoretical predictions such as the ones in this work.

4 | Conclusions

In this work, we employ MD simulations with a ML-FF to investigate the effect of the nanoparticle–support interaction including azimuthal orientation on the particle melting. We find that applying constraints to facets or edges consistently hinders NP melting to higher temperatures. This effect is more pronounced for smaller NPs, whereas for larger NPs, the melting temperatures of free and constrained particles are much closer. The landing orientation of the supported NPs plays a significant role: constraining the (100) facet results in a greater melting point depression than constraining the (111) facet, despite the (100) facet being smaller in these NPs. Importantly, the degree of the melting increase is independent of the interaction strength with the support. Thus, NP melting is expected to be significantly hindered even under all kinds of support interactions. We believe these results provide a framework for more accurate predictions of the melting temperatures of sub-4 nm metal NPs in practical applications and under operational conditions. Similar conclusions could be drawn for the other PGM metals, which share the same crystal structure with Au. An investigation following the same methodology but focusing on NPs of other crystal structures and a comparison of the melting mechanics would be of great interest. Future works could also extend the methodology by applying springs of different k constants on each atomic layer and/or by investigating scenarios where the NPs are embedded deep in the support material.

Author Contributions

Th. Pavloudis: conceptualization (equal), data curation (lead), formal analysis (equal), investigation (lead), methodology (equal), resources (equal), supervision (equal), validation (lead), visualization (equal), writing – original draft (equal), writing – review and editing (lead). **C. Gennetidis:** formal analysis (equal), visualization (equal), writing – original draft (equal). **J. Kioseoglou:** conceptualization (equal), methodology (equal), resources (equal), supervision (equal), writing – review and editing (supporting). **R. E. Palmer:** conceptualization (equal), methodology (equal), project administration (lead), resources (equal), writing – review and editing (supporting).

Acknowledgments

Computational resources were provided by the Greek Research & Technology Network (GRNET) in the "ARIS" National HPC infrastructure under the project NOUS (017012), the project DataMind (555141862428) of AWS, and the Supercomputing Wales project, which is part-funded by the European Regional Development Fund (ERDF) via Welsh Government.

Conflicts of Interest

The authors declare no conflicts of interest.

Data Availability Statement

The data that support the findings of this study are available from the corresponding author upon reasonable request.

References

1. D. Astruc, "Introduction: Nanoparticles in Catalysis," *Chemical Reviews* 120, no. 2 (2020): 461–463, https://doi.org/10.1021/acs.chemrev.8b00696.

2. M. Haruta, T. Kobayashi, H. Sano, and N. Yamada, "Novel Gold Catalysts for the Oxidation of Carbon Monoxide at a Temperature Far Below 0°C," *Chemistry Letters* 16, no. 2 (1987): 405–408, https://doi.org/10.1246/cl.1987.405.

3. P. Pawlow, "Ober Die Abhängigkeit Des Schmelzpunktes Von der Oberflächenenergie Eines Festen Körpers (Zusatz)," *Zeitschrift Für Physikalische Chemie* 65U, no. 1 (1909): 545–548, https://doi.org/10.1515/zpch-1909-6532.

4. H. Reiss and I. B. Wilson, "The Effect of Surface on Melting Point," *Journal of Colloid Science* 3, no. 6 (1948): 551–561, https://doi.org/10.1016/s0095-8522(48)90048-8.

5. K.-J. Hanszen, "Theoretische Untersuchungen über Den Schmelzpunkt Kleiner kügelchen," *Zeitschrift fPhysik* 157, no. 5 (1960): 523–553, https://doi.org/10.1007/bf01340711.

6. A. E. Curzon. Ph.D. Dissertation, *Imperial College, University of London* (1959).

7. J. R. Sambles, "An Electron Microscope Study of Evaporating Gold Particles: The Kelvin Equation for Liquid Gold and the Lowering of the Melting Point of Solid Gold Particles," *Proceedings of the Royal Society of London. Series A, Mathematical and Physical Sciences* 324, no. 1558 (1971): 339–351, http://www.jstor.org/stable/78060.

8. P. R. Couchman and W. A. Jesser, "Thermodynamic Theory of Size Dependence of Melting Temperature in Metals," *Nature* 269, no. 5628 (1977): 481–483, https://doi.org/10.1038/269481a0.

9. P. Schlexer, A. B. Andersen, B. Sebok, I. Chorkendorff, J. Schiøtz, and T. W. Hansen, "Size-Dependence of the Melting Temperature of Individual Au Nanoparticles," *Particle & Particle Systems Characterization* 36, no. 3 (2019): 1800480, https://doi.org/10.1002/ppsc.201800480.

10. S. Hu, K.-J. Hu, Z. Zhao, et al., "In Situ Heating Characterization of Structural Evolution and Size-Dependent Melting Point Depression in Gold Nanoclusters: A Comprehensive Thermodynamic Investigation," *Nanoscale* 16, no. 39 (2024): 18399–18409, https://doi.org/10.1039/d4nr02111h.

11. D. M. Foster, Th Pavloudis, J. Kioseoglou, and R. E. Palmer, "Atomic-Resolution Imaging of Surface and Core Melting in Individual Size-Selected Au Nanoclusters on Carbon," *Nature Communications* 10, no. 1 (2019): 2583, https://doi.org/10.1038/s41467-019-10713-z.

12. V. M. Samsonov, I. V. Talyzin, S. A. Vasilyev, V. V. Puytov, and A. A. Romanov, "On Surface Pre-Melting of Metallic Nanoparticles: Molecular Dynamics Study," *Journal of Nanoparticle Research* 25, no. 6 (2023): 105, https://doi.org/10.1007/s11051-023-05743-0.

13. L. Liu and A. Corma, "Metal Catalysts for Heterogeneous Catalysis: From Single Atoms to Nanoclusters and Nanoparticles," *Chemical Reviews* 118, no. 10 (2018): 4981–5079, https://doi.org/10.1021/acs.chemrev.7b00776.

14. K. Rossi, T. Mineva, J.-S. Filhol, F. Tielens, and H. Guesmi, "Realistic Modelling of Dynamics at Nanostructured Interfaces Relevant to Heterogeneous Catalysis," *Catalysts* 12, no. 1 (2022): 52, https://doi.org/10.3390/catal12010052.

15. A. C. Ngandjong, C. Mottet, and J. Puibasset, "Freezing and Melting of Silver Nanoparticles on Silica Substrate Using a Simple Interatomic Potential for Ag–SiO_2 Interaction on the Basis of Ab Initio Calculations and Experimental Data," *The Journal of Physical Chemistry C* 121, no. 6 (2017): 3615–3622, https://doi.org/10.1021/acs.jpcc.6b12084.

16. K. Rossi, T. Ellaby, L. O. Paz-Borbón, I. Atanasov, L. Pavan, and F. Baletto, "Melting of Large Pt@MgO(100) Icosahedra," *Journal of Physics: Condensed Matter* 29, no. 14 (2017): 145402, https://doi.org/10.1088/1361-648x/aa5a1d.

17. B. H. Morrow and A. Striolo, "Platinum Nanoparticles on Carbonaceous Materials: The Effect of Support Geometry on Nanoparticle Mobility, Morphology, and Melting," *Nanotechnology* 19, no. 19 (2008): 195711, https://doi.org/10.1088/0957-4484/19/19/195711.

18. C. Qiu, C. Zhao, X. Sun, et al., "Multiscale Simulation of Morphology Evolution of Supported Pt Nanoparticles via Interfacial Control," *Langmuir : the Acs Journal of Surfaces and Colloids* 35, no. 19 (2019): 6393–6402, https://doi.org/10.1021/acs.langmuir.9b00129.

19. G. Mahmud, H. Zhang, and J. F. Douglas, "The Dynamics of Metal Nanoparticles on a Supporting Interacting Substrate," *The Journal of Chemical Physics* 157, no. 11 (2022): 114505, https://doi.org/10.1063/5.0105208.

20. H. Eliasson, Y. Niu, R. E. Palmer, H. Grönbeck, and R. Erni, "Support-Facet-Dependent Morphology of Small Pt Particles on Ceria," *Nanoscale* 15, no. 47 (2023): 19091–19098, https://doi.org/10.1039/d3nr04701f.

21. T. Maxson and T. Szilvási, "Metal-Support Interactions Reshape Nanoparticle Catalyst Surfaces," *Angewandte Chemie Novit* 1, no. 1 (2025): e70008, https://doi.org/10.1002/anov.70008.

22. T. Ishida, T. Murayama, A. Taketoshi, and M. Haruta, "Importance of Size and Contact Structure of Gold Nanoparticles for the Genesis of Unique Catalytic Processes," *Chemical Reviews* 120, no. 2 (2020): 464–525, https://doi.org/10.1021/acs.chemrev.9b00551.

23. W. Wu, A. V. Verkhovtsev, T. Pavloudis, A. V. Solov'yov, and R. E. Palmer, "Neuromorphic Nanocluster Networks: Critical Role of the Substrate in Nano-Link Formation," *Nano Research* 16, no. 7 (2023): 10500–10506, https://doi.org/10.1007/s12274-023-5744-5.

24. S. Lethbridge, T. Pavloudis, J. McCormack, T. Slater, J. Kioseoglou, and R. E. Palmer, "Stabilization of 2D Raft Structures of Au Nanoclusters with up to 60 Atoms by a Carbon Support," *Small Science* 4, no. 8 (2024): 2400093, https://doi.org/10.1002/smsc.202400093.

25. P. Kraszkiewicz, M. Małecka, and W. Mišta, "Sintering-Resistant and Highly Active Au/SBA-15 Catalyst for Carbon Monoxide Oxidation," *Microporous and Mesoporous Materials* 346 (2022): 112338, https://doi.org/10.1016/j.micromeso.2022.112338.

26. C. Zeni, K. Rossi, T. Pavloudis, et al., "Data-Driven Simulation and Characterisation of Gold Nanoparticle Melting," *Nature Communications* 12, no. 1 (2021): 6056, https://doi.org/10.1038/s41467-021-26199-7.

27. A. P. Thompson, H. M. Aktulga, R. Berger, et al., "LAMMPS - a Flexible Simulation Tool for Particle-Based Materials Modeling at the Atomic, Meso, and Continuum Scales," *Computer Physics Communications* 271 (2022): 108171, https://doi.org/10.1016/j.cpc.2021.108171.

28. J. Vandermause, S. B. Torrisi, S. Batzner, et al., "On-the-Fly Active Learning of Interpretable Bayesian Force Fields for Atomistic Rare Events," *NPJ Computational Materials* 6, no. 1 (2020): 20, https://doi.org/10.1038/s41524-020-0283-z.

29. J. P. Perdew and A. Zunger, "Self-Interaction Correction to Density-Functional Approximations for Many-Electron Systems," *Physical Review B* 23, no. 10 (1981): 5048–5079, https://doi.org/10.1103/physrevb.23.5048.

30. B. Hammer, L. B. Hansen, and J. K. Nørskov, "Improved Adsorption Energetics Within Density-Functional Theory Using Revised Perdew-Burke-Ernzerhof Functionals," *Physical Review B* 59, no. 11 (1999): 7413–7421, https://doi.org/10.1103/physrevb.59.7413.

31. T. Pavloudis, J. Kioseoglou, and R. E. Palmer, "Bonding of Gold Nanoclusters on Graphene with and without Point Defects," *Nanomaterials* 10, no. 11 (2020): 2109, https://doi.org/10.3390/nano10112109.

32. V. M. Samsonov, S. A. Vasilyev, K. K. Nebyvalova, et al., "Melting Temperature and Binding Energy of Metal Nanoparticles: Size Dependences, Interrelation between Them, and Some Correlations with Structural Stability of Nanoclusters," *Journal of Nanoparticle Research* 22, no. 8 (2020): 247, https://doi.org/10.1007/s11051-020-04923-6.

33. L. Delgado-Callico, K. Rossi, R. Pinto-Miles, P. Salzbrenner, and F. Baletto, "A Universal Signature in the Melting of Metallic Nanoparticles," *Nanoscale* 13, no. 2 (2021): 1172–1180, https://doi.org/10.1039/d0nr06850k.

34. J. Dana Honeycutt and H. C. Andersen, "Molecular Dynamics Study of Melting and Freezing of Small Lennard-Jones Clusters," *The Journal of Physical Chemistry* 91, no. 19 (1987): 4950–4963, https://doi.org/10.1021/j100303a014.

35. A. Stukowski, "Structure Identification Methods for Atomistic Simulations of Crystalline Materials," *Modelling and Simulation in Materials Science and Engineering* 20, no. 4 (2012): 045021, https://doi.org/10.1088/0965-0393/20/4/045021.

36. A. Stukowski, "Visualization and Analysis of Atomistic Simulation Data with OVITO–the Open Visualization Tool,"*Modelling and Simulation in Materials Science and Engineering* 18, no. 1 (2010): 015012, https://doi.org/10.1088/0965-0393/18/1/015012.

37. D. Nelli, G. Rossi, Z. Wang, R. E. Palmer, and R. Ferrando, "Structure and Orientation Effects in the Coalescence of Au Clusters," *Nanoscale* 12, no. 14 (2020): 7688–7699, https://doi.org/10.1039/c9nr10163b.

38. G. Guenther and O. Guillon, "Models of Size-Dependent Nanoparticle Melting Tested on Gold," *Journal of Materials Science* 49, no. 23 (2014): 7915–7932, https://doi.org/10.1007/s10853-014-8544-1.

Supporting Information

Additional supporting information can be found online in the Supporting Information section. **Supporting Fig. S1:** (a) An Au_{561} cuboctahedral NP. (b) The energies per atom of Au NPs vs their size. **Supporting Fig. S2:** (a) A Au atom on a graphene vacancy and (b) the force along the axis. **Supporting Fig. S3:** The average force along the axis on the atoms of each layer of an Au_{561} cuboctahedral NP with its (111) facet on graphene. Data from DFT simulations from Ref. [8]. **Supporting Fig. S4:** The critical radius extracted from the simulations vs. the NP size. **Supporting Table S1:** Constrained atoms for each model NP. **Supporting Table S2:** The diameters and radii of icosahedral quasi-spherical NPs. **Supporting Table S3:** The diameters and radii of quasi-spherical NPs with atoms of the NPs investigated in this work. **Supporting Table S4:** Constants used for plotting the melting models in Figure 6. The values were copied from the SI of Ref. [8].